3D inversion of regional MT data distorted by near-surface inhomogeneities using a complex distortion matrix

Alexander Gribenko and Michael S. Zhdanov, University of Utah, TechnoImaging, and MIPT*

SUMMARY

The distortion of regional electric fields by local structures represents one of the major problems facing three-dimensional magnetotelluric (MT) interpretation. The effect of 3D local inhomogeneities on MT data can be described by a distortion matrix. In this paper, we develop a method for simultaneous inversion of the full MT impedance data for 3D conductivity distribution and for a distortion matrix with complex components. We use integral equations method for forward modeling. Tikhonov regularization is employed to solve the resulting inverse problem. Minimization of the parametric functional is achieved via a conjugate gradient method. The inversion algorithm was tested on the synthetic data from Dublin Secret Model II (DSM 2), for which multiple inversion solutions are available for comparison. We also investigate a possibility of using the developed approach for corrections to the effect of topography on the MT data. Finally, the results are presented of an application of the inversion to a regional MT dataset acquired as part of the EarthScope project over the Great Basin region of the Western United States.

INTRODUCTION

Distortion of regional MT responses by local structures is one of the challenges in the interpretation of MT data. Due to the computing limitations it is difficult to model local 3D structures to a small enough scale. There are several approaches available for minimizing static shift effects. For example, one can use additional data produced by the controlled source EM surveys, e.g., coincident time-domain EM soundings (Pellerin and Hohmann, 1990). Torres-Verdin and Bostick (1992) proposed the EMAP technique of deploying electric dipoles along a continuous survey path to reduce the static shift effect in the data. In the paper by deGroot-Hedlin (1991), the unknown static shift was included as a parameter of the inversion. The 3D MT inversion algorithm of Sasaki and Meju (2006) took into account the static shift of the impedance amplitudes but not amplitude or phase mixing. Zhdanov et. al. (2011) normalized observed MT impedances by their amplitudes in order to remove the major part of the static shift effect from the amplitude data, considering that the phase of impedances is less affected by near-surface inhomogeneities. Patro et al. (2013) presented an inversion algorithm for the MT phase tensor, which was based on a similar assumption of the lesser influence of near-surface distortions on the phase data.

Groom and Bailey (1989) introduced a widely accepted method of decomposition of the MT impedance tensor in the presence of local 3D inhomogeneities, which can be formally represented as a product of the undisturbed impedance tensor and a distortion matrix:

$$\mathbf{Z}^{obs} = \mathbf{c}\mathbf{Z}^{und}, \tag{1}$$

where $\mathbf{Z}^{obs}$ is the observed impedance tensor,

$$\mathbf{Z}^{obs} = \begin{bmatrix} Z_{xx}^{obs} & Z_{xy}^{obs} \\ Z_{yx}^{obs} & Z_{yy}^{obs} \end{bmatrix}, \tag{2}$$

$\mathbf{c}$ is the distortion matrix,

$$\mathbf{c} = \begin{bmatrix} c_{11} & c_{12} \\ c_{21} & c_{22} \end{bmatrix}, \tag{3}$$

and $\mathbf{Z}^{und}$ is the undisturbed impedance tensor,

$$\mathbf{Z}^{und} = \begin{bmatrix} Z_{xx}^{und} & Z_{xy}^{und} \\ Z_{yx}^{und} & Z_{yy}^{und} \end{bmatrix}. \tag{4}$$

The papers by Miensopust (2009) and Avdeeva et al. (2012) introduced 3D joint inversion of the impedance tensor and distortion matrix with the real components. Baba et al. (2013) assumed a distortion matrix with complex components in an attempt to account for bathymetry effects in a marine magnetotelluric survey. Our general approach differs from Avdeeva et al. (2012) in that we invert for complex distortion matrix. This allows us to take into account not only the conventional DC static shift but also possible phase changes of the impedance tensor. We use the regularized conjugate gradient method (Zhdanov, 2002), which considerably reduces computer memory requirements compared to direct solution methods. Further memory savings are provided by consideration of variable sensitivity domains for different frequencies and receivers based on corresponding skin depths (Zhdanov et. al. , 2010, 2011, 2012). We use the integral equation forward modeling method (Hohmann, 1975), which not only provides an accurate solution of the forward problem, but also supplies straightforward approximate expression for the Fréchet derivative (sensitivity) matrix without any additional forward modeling required. The inversion method was applied to the DSM2 synthetic data. The resulting inverse model was in good agreement with the true model (Miensopust et al., 2013). In our opinion, the result provided by our inversion is superior to most results presented in Miensopust et al. (2013).

The MT method is one of a few geophysical methods capable of imaging the regional structures of the Earth's crust and upper mantle. The Great Basin region of the Western United States has a rich tectonic history and is undergoing an extensional deformation at the present time. We applied our inversion to the MT data collected over the Great Basin as part of the EarthScope project. The results of inversion outline the areas of increased conductivity, which correspond to areas of active tectonism and potential geothermal reservoirs.

PRINCIPLES OF MT INVERSION WITH A COMPLEX DISTORTION MATRIX

Taking into account decomposition 1, the forward MT problem can be written in operator notations as follows:

$$\mathbf{d} = \mathbf{c}\mathbf{Z}^{und} = \mathbf{c}\,\mathbf{A}(\sigma), \tag{5}$$

where $\mathbf{d}$ stands for the observed MT impedance data, $\mathbf{Z}^{obs}$, recorded in the receivers; $\mathbf{A}$ is a forward modeling operator based on IE formulation, which is used to compute the undisturbed impedance $\mathbf{Z}^{und}$; and σ is a vector of the anomalous conductivity distribution within the inversion domain. In order to find the conductivity distribution and the distortion matrix from the observed MT impedances, we follow the standard Tikhonov regularization procedure (Tikhonov and Arsenin, 1977; Zhdanov, 2002) of constructing a parametric (cost) functional:

$$P(\sigma,\mathbf{c}) = \|\mathbf{r}\|^2 + \alpha\,\|\mathbf{S}\|^2, \tag{6}$$

$$\mathbf{r} = \mathbf{W}_d\,(\mathbf{c}\mathbf{A}(\sigma) - \mathbf{d}), \tag{7}$$

$$\mathbf{S} = \mathbf{W}_m \begin{bmatrix} \mathbf{S}_\sigma \\ \mathbf{S}_\mathbf{c} \end{bmatrix} = \mathbf{W}_m \begin{bmatrix} \mathbf{L}(\sigma - \sigma_b) \\ (\mathbf{c} - \mathbf{c}_0) \end{bmatrix}, \tag{8}$$

where $\mathbf{W}_d$ and $\mathbf{W}_m$ are the data and model weighting matrices, respectively; σ_b is a vector of the reference conductivity distribution; $\mathbf{L}$ is a matrix of the finite difference operator, $\mathbf{c}_0$ is an priori distortion matrix, selected as a 2x2 identity matrix, which represents the case with no distortion. The regularization parameter α balances the effect of the misfit and stabilizing functionals and is selected using the adaptive regularization as described below. The data weights are computed as the inverse of the noise levels (variances) for the corresponding data points. If the noise level is unknown, 3.5% of the value of the principal impedances for a given station and frequency is used for all components. The model weighting matrix, $\mathbf{W}_m$, is calculated based on the integrated sensitivity as follows (Zhdanov, 2002):

$$\mathbf{W}_m = diag(\mathbf{F}^T\mathbf{F})^{1/4}, \tag{9}$$

where $\mathbf{F}$ is a Fréchet derivative (sensitivity) matrix of the forward modeling operator.

We use preconditioned conjugate gradient method with a linear line search (Nocedal and Wright, 1999) to minimize parametric functional 7. The inverse of the squared model weighting matrix 9 is used as the preconditioner, $\mathbf{P}$:

$$\mathbf{P} = \left(\mathbf{W}_m^T\mathbf{W}_m\right)^{-1}. \tag{10}$$

Application of a gradient method to a nonlinear inverse problem, such as minimization of the parametric functional 7, requires calculation of a Fréchet derivative or sensitivity matrix, $\mathbf{F}$. A direct "brute force" calculation of the sensitivity matrix using the finite-difference method requires multiple additional forward modeling solutions. One of the advantages of using the IE method as a forward modeling engine is that an approximate but accurate Fréchet derivative $\mathbf{F}$ with respect to the conductivity is readily available from the solution of the forward modeling problem (Gribenko and Zhdanov, 2007):

$$\mathbf{F}_\sigma^{E,H} = \frac{\delta\mathbf{E},\mathbf{H}}{\delta\Delta\sigma} = \mathbf{G}_{E,H}\mathbf{E}_D. \tag{11}$$

This approximation of the Fréchet derivative is called quasi-Born due to its similarity to the classical Born approximation, where instead of the total electric field the background field is used. A simple chain rule is applied to obtain the Fréchet derivatives of the impedance components once the derivatives of the EM field components are computed (Zhdanov, 2009). The Fréchet derivatives of impedances $Z_{\alpha\beta}^{obs}$ with respect to the components of the distortion matrix c_{ij} can be obtained directly from equation 1, for example

$$\mathbf{F}_{c_{11}}^{Z_{xx}^{obs}} = \frac{\delta\left(c_{11}Z_{xx}^{und} + c_{12}Z_{yx}^{und}\right)}{\delta c_{11}} = Z_{xx}^{und}. \tag{12}$$

The code was written in the MatLab(R) language. All inversions were performed on a 12-core Intel(R) Xeon(R) X5690 @ 3.47 GHz with 192 GB of RAM available, running Red Hat Enterprise Linux release 6.4. The MatLab(R) version was R2014a with the parallel computing toolbox. Calculations of Greens' tensors and Fréchet derivatives were parallelized over frequencies using the toolbox. The IE forward problem was solved via the PIE3D v.2012 code. The PIE3D is a parallel EM forward modeling software based on the IE method. The PIE3D ver. 2012 is portable on any computer that supports message passing interface (MPI). This code simulates frequency-domain EM responses of 3D anomalous conductivity structures located within a horizontally layered medium (Zhdanov et al., 2006; Cuma and Zhdanov, 2013).

DUBLIN SECRET MODEL 2

We applied the algorithm described above to the DSM2 data available from:
http://www.dias.ie/mt3dinv2/3D_inversion_test_data_set.html (last accessed 26 August, 2013). This data set was used at the 2nd MT inversion workshop to test and compare results of different 3D inversion codes. The results of comparison were thoroughly reviewed in Miensopust et al. (2013). Unlike the workshop participants, we had an advantage of knowing the model for which the data were computed. Nevertheless, inverting the data posed a challenging problem due to the amount of data, range of frequencies, and data corruption from noise. DSM 2 model is a modified version of the COMMEMI 3D-2A model of Zhdanov et al. (1997). The random galvanic distortions were applied to the synthetic data set. The distortion matrix C was calculated according to the Groom–Bailey Decomposition (Groom and Bailey, 1989) from randomly generated values for the twist angle (within $\pm 60^o$), the shear angle (within $\pm 45^o$) and the anisotropy (within ± 1). The gain value was fixed to be equal to one at all locations. Finally, random Gaussian noise of 5 percent of the maximum impedance value was applied to the distorted data set (Miensopust et al., 2013). 144 MT stations were included in the synthetic survey. The data were provided as a set of 30 periods from 0.0158 to 10,000 sec. Our inversion code is parallelized over periods, and runs most efficiently when the number of periods is a multiple of the number of available processors (12). Therefore, the data were interpolated on a new set of 24 logarithmically spaced periods from 0.04 to 10,000 sec. All 144 stations were included in the

inversion. The result of 1D inversion of the sounding curve averaged over all stations was used as the initial model for 3D inversion. The size of the inversion domain was 80 x 80 x 37.76 km^3. This domain was discretized into 76,800 inversion cells with a horizontal cell size of 2 x 2 km^2. We used 48 horizontal layers with thicknesses increasing logarithmically from 200 m to 2,000 m.

We first applied conductivity-only inversion to the DSM 2 dataset. The conversion stopped at RMS error of 6.66 after 851 total iterations with 43 rigorous updates, taking approximately 16 hours of CPU time. We run conductivity-only inversion until the RMS error had changed less than 1% between the rigorous iterations. For the DSM 2 inversion the change occurred at an RMS value of 6.90 after 101 total iterations with 4 rigorous updates. A complex distortion matrix was introduced in the inversion at this point. The RMS reached 1.35 and stopped changing after 1,606 total iterations with 28 rigorous updates, including conductivity-only iterations, taking approximately 9 hours. The most striking difference between the two inversions, conductivity-only and with the distortion matrix, can be seen in the levels of the data misfit. The joint inversion provides a close to perfect RMS error of 1.35. Figure 1 illustrates the data fit for both conductivity-only and joint inversions. This figure shows the values of the RMS errors at each station as well as examples of the observed and predicted MT sounding curves.

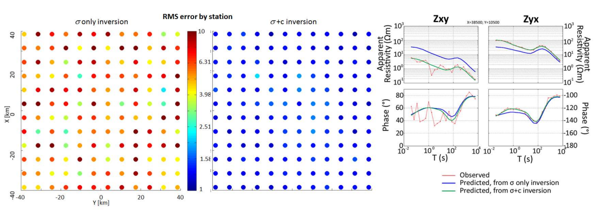

Figure 1: A comparison of the data fit. The left panel shows the distribution of the RMS errors for the conductivity-only inversion. The central panel presents the RMS errors for joint inversion. The right panel presents examples of observed and predicted MT sounding curves for one of the stations.

Figure 2 compares conductivity distributions for the true model, the results of the conductivity-only inversion, and the result of a joint inversion for conductivity and the complex distortion matrix. The results of both inversions provide a very reasonable representation of the true model. The joint inversion produces a more accurate estimate of the depth of the bottom of the conductive layer as well as the shape and resistivity of the resistor appearing in the top layer. These features of the model have small overall effect on the observed data, and cannot be recovered by conductivity-only inversion due to strong regularization. In this case, regularization parameter α remains relatively high throughout the inversion process due to high level of the data misfit. It is apparent that the data cannot be fitted with high accuracy without adding distortions as inversion parameters. On the other hand, the joint inversion reaches the lower level of the misfit, which results in the smaller values of the regularization parameter. The more relaxed regularization results in the less smooth conductivity image.

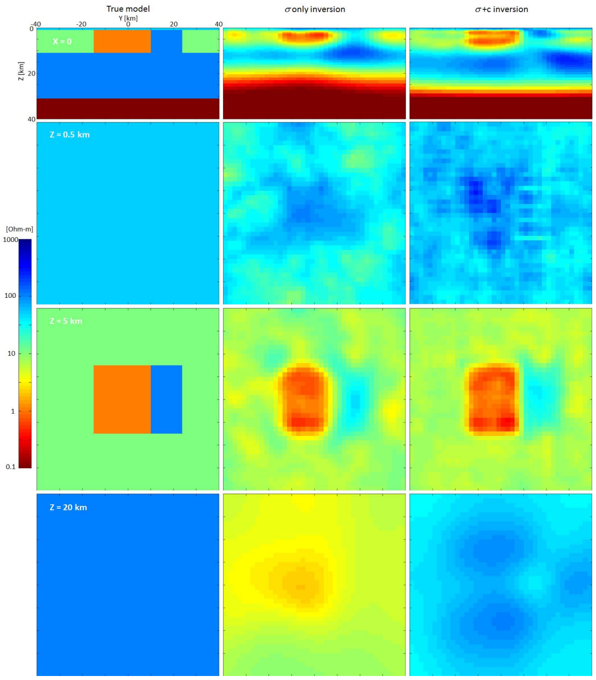

Figure 2: DSM 2 conductivity distributions. The left column shows the true model. The middle column presents the results of the conductivity only inversion. The right column shows the results of the joint inversion for the conductivity and distortion matrix.

The real and imaginary components of the distortion tensor are shown in Figure 3. The DSM 2 data were contaminated with random distortions represented by the real numbers. Note that, the inversion for the complex components of the distortion matrix did not introduce complex distortions; the values of the imaginary parts are negligibly small compared to the real parts of the components of the distortion matrix. This fact confirms the suggestion made by Zhdanov et. al. (2011) that the phase of the impedances is less affected by the near-surface inhomogeneities than their amplitude. Significant values of the off-diagonal distortion components indicate that amplitude and phase mixing is present in the observed data.

GREAT BASIN DATA INVERSION

For a real data example we selected a subset of the MT data collected as a part of the EarthScope project over the Great Basin region of the Western United States (www.earthscope.org). The MT data used at this example were collected in 98 sites distributed approximately 80 km apart over 1000 km x 500 km area covering parts of California, Oregon, Nevada, Idaho, Utah, and Wyoming. The original data contained 30 periods ranging from 7.3153 to 18,724 sec. The impedance data were interpolated on 24 log-spaced periods from 10 to 10,000 sec. Minimal data cleaning resulted in the removal of 48 impedance values out of 11,400.

The inversion domain was extended 650 km in the X (North-

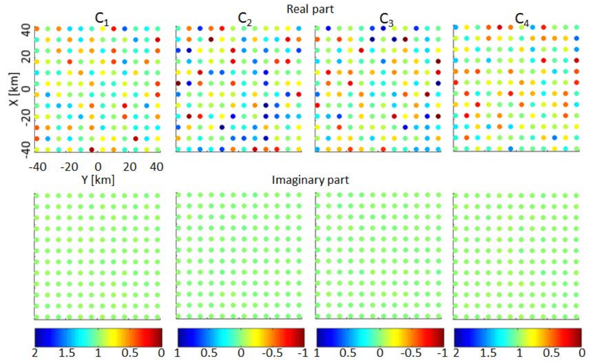

Figure 3: DSM 2 distortion distribution. The circles correspond to the receiver locations. The top row shows the real parts of the distortion,while the bottom row presents the imaginary parts. The four columns correspond to the four components of the distortion matrix.

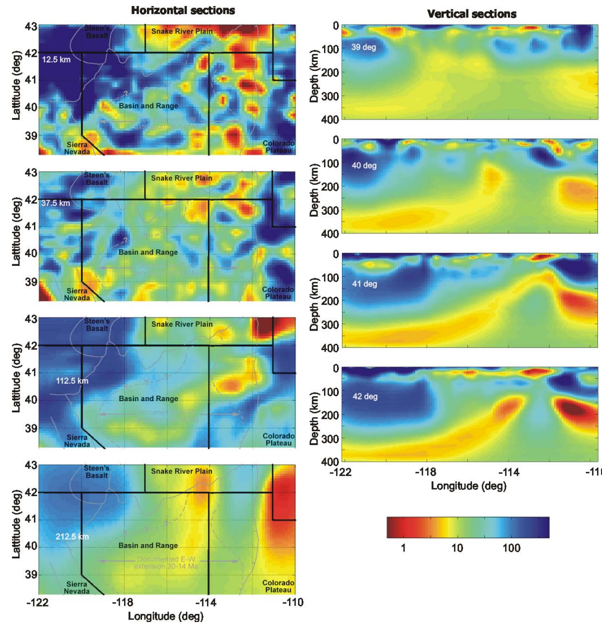

Figure 4: The horizontal (left) and vertical (right) sections of the inversion result for the Great Basin MT data. The gray boundaries in the plan views outline the Cenozoic tectonic provinces (Colgan et. al., 2006), the Steens Basalts (Hooper et al., 2002), and an approximate contour of 30–15 Ma Basin and Range extension (Dilles and Gans, 1995).

South) direction, 1150 km in the Y (East-West), and 308.2 km in the vertical direction. The horizontal cell size was kept at a constant size at 10×10 km^2, while the thicknesses of the cells increased from 1 to 20 km logarithmically for a total number of 48 layers. Figure 4 shows horizontal and vertical sections of the inversion result. Several geological provinces show distinct conductivity anomalies. The Great Basin province is characterized by the regions of elevated conductivity at relatively low depths of around 100 km or less, bounded by resistive Colorado Plateau to the East and the Sierra Nevada mountains to the West. There is a prominent conductive region at the eastern edge of the Great Basin province along the Wasatch Fault at shallow depths. The Snake River plain is also characterized by higher conductivity. It appears that the boundaries of the 15 - 30 Ma Basin and Range extension may have a conductivity signature at a depth of about 200 km.

CONCLUSIONS

We have developed a 3D MT inversion algorithm which takes into account the effect of 3D local inhomogeneities on the MT data by introducing in the inversion scheme the unknown components of the distortion matrix jointly with the unknown conductivity. In order to provide more flexibility for the inversion, the components of the distortion matrix were allowed to be complex. The inversion algorithm is based on the rigorous IE forward modeling method and regularized conjugate gradient optimization.

The developed inversion code was successfully applied to the synthetic data from Dublin Secret Model II (DSM 2) with significant distortion and noise levels. We also tested the feasibility of the method for removal of the topography effect from the MT data. Application of this MT inversion algorithm to real data from the Great Basin region of the Western US revealed conductivity anomalies which agreed well with major geological provinces of the area. From the topography model study we concluded that allowing the nonzero imaginary part of the components of the distortion matrix helped to minimize the topography effect. At the same time, both the model and case studies demonstrated that the imaginary part of the distortion matrix components was typically significantly smaller than the real part. This observation confirms the well established fact that the phase of impedances is less affected by the near-surface inhomogeneities than their amplitude. Significant values of the off-diagonal distortion matrix components verify that amplitude and phase mixing are present in realistic 3D situations.

ACKNOWLEDGEMENTS

The authors would like to thank Virginia Maris for helpful discussions. We acknowledge the support of the Consortium for Electromagnetic modeling and Inversion (CEMI) at the University of Utah and TechnoImaging LLC. The MT data were acquired by the Incorporated Research Institutions for Seismology (IRIS) as part of the operation of the USArray. Data used in this study were made available through Earth-Scope (www.earthscope.org; EAR-0323309), supported by the National Science Foundation.

Avdeeva, A., M. Moorkamp, and D. Avdeev, 2012, Three-dimensional joint inversion of magnetotelluric impedance tensor data and full distortion matrix: 21st EM induction workshop, Extended Abstracts, S3.5.

Baba, K., N. Tada, H. Utada, and W. Siripunvaraporn, 2013, Practical incorporation of local and regional topography in three-dimensional inversion of deep ocean magnetotelluric data.: Geophysical Journal International, doi: 10.1093/gji/ggt115.

Colgan, J. P., T. A. Dumitru, P. W. Reiners, J. L. Wooden, and E. L. Miller, 2006 Cenozoic Tectonic Evolution of the Basin and Range Province in Northwestern Nevada, American Journal of Science, **306**(8), 616-654.

Čuma, M., and M. S. Zhdanov, 2013, The PIE3D ver. 2012: Consortium for Electromagnetic Modeling and Inversion annual meeting, CEMI, Expanded Abstracts, 321-322.

deGroot-Hedlin, C., 1991, Removal of static shift in two dimensions by regularized inversion: Geophysics, **56**, 2102-2106.

Dilles, J. H., and P. B. Gans, 1995, The chronology of Cenozoic volcanism and deformation in the Yerington area, western Basin and Range and Walker Lane: Geological Society of America Bulletin, **107**(4), 474-486.

Gribenko, A. and M. S. Zhdanov, 2007, Rigorous 3D inversion of marine CSEM data based on integral equation method: Geophysics, **72** (2), WA73-WA84.

Groom, R. W., and R. C. Bailey, 1989, Decomposition of magnetotelluric impedance tensors in the presence of local three dimensional galvanic distortion, Journal of Geophysical Research, **94**, 1913-1925.

Hohmann, G. W., 1975, Three-dimensional induced polarization and electromagnetic modeling: Geophysics, **40**, 309-324.

Hooper, P. R., G. B. Binger, and K. R. Lees, 2002, Ages of the Steens and Columbia River flood basalts and their relationship to extension-related calc-alkalic volcanism in eastern Oregon: Geological Society of America Bulletin, **114**, 43-50

Miensopust, M. P., 2009, Multidimensional magnetotellurics: A 2D case study and a 3D approach to simultaneously invert for resistivity structure and distortion parameters: Ph.D. thesis, National University of Ireland, Galway.

Miensopust, M. P., Queralt, P., Jones, A. G., and the 3D modellers, 2013, Magnetotelluric 3-D inversion - a review of two successful workshops on forward and inversion code testing and comparison: Geophysical Journal International, **193** (3), 1216-1238.

Nocedal, J., and S. J. Wright, 1999, Numerical Optimization: Springer.

Patro, P. K., M. Uyeshima, and W. Siripunvaraporn, 2013, Three-dimensional inversion of magnetotelluric phase tensor data: Geophysical Journal International, **192**, 58-66.

Pellerin, L., and G. W. Hohmann, 1990, Transient electromagnetic inverison: A remedy for magnetotelluric static shifts: Geophysics, **55**, 1242-1250.

Sasaki, Y., and M. A. Meju, 2006, Three-dimensional joint inversion for magnetotelluric resistivity and static shift distributions in complex media: Journal of Geophysical Research, **111**, B05101.

Tikhonov, A. N., and V. Y. Arsenin, 1977, Solution of ill-posed problems: Winston & Sons.

Torres-Verdin, C., and F.X. Bostick, 1992, Principles of spatial surface electric field filtering in magnetotellurics: Electromagnetic array profiling (EMAP): Geophysics, **57**, 603-622.

Zhdanov, M. S., 2002, Geophysical inverse theory and regularization problems: Elsevier.

Zhdanov, M. S., 2009, Geophysical electromagnetic theory and methods: Elsevier.

Zhdanov, M. S., I. M. Varentsov, J. T. Weaver, N. G. Golubev, and V.A. Krylov, 1997, Methods for modelling electromagnetic fields Results from COMMEMI—the international project on the comparison of modelling methods for electromagnetic induction: Journal of Applied Geophysics, **37**, 133-271.

Zhdanov, M. S., S. K. Lee, and K. Yoshioka, 2006, Integral equation method for 3D modeling of electromagnetic fields in complex structures with inhomogeneous background conductivity, Geophysics, **71**, G333-G345.

Zhdanov, M. S., M. Green, A. Gribenko, and M. Cuma, M., 2010, Large-scale three-dimensional inversion of Earthscope MT data using the integral equation method: Fizika Zemli, 8, 27-35.

Zhdanov, M. S., R. B. Smith, A. Gribenko, M. Cuma, and M. Green, 2011, Three-dimensional inversion of large-scale EarthScope magnetotelluric data based on the integral equation method: Geoelectrical imaging of the Yellowstone conductive mantle plume: Geophysical Research Letters, **38**, L08307.

Zhdanov, M. S., A. Gribenko, M. Cuma, and M. Green, 2012, Geoelectrical structure of the lithosphere and asthenosphere beneath the Northwestern United States: Journal of Geology and Geosciences, **1** (2), 1000106, 1-6.